Temperature-dependent equilibration of spin orthogonal quantum Hall edge modes

Tanmay Maiti,[1,*] Pooja Agarwal,[1] Suvankar Purkait,[1] G. J. Sreejith,[2] Sourin Das,[3] Giorgio Biasiol,[4] Lucia Sorba,[5] and Biswajit Karmakar[1]

[1]*Saha Institute of Nuclear Physics, HBNI, 1/AF Bidhannagar, Kolkata 700064, India*
[2]*Indian Institute of Science Education and Research, Pune 411008, India*
[3]*Department of Physical Sciences, IISER Kolkata, Mohanpur, West Bengal 741246, India*
[4]*Istituto Officina dei Materiali CNR, Laboratorio TASC, 34149 Trieste, Italy*
[5]*NEST, Istituto Nanoscienze-CNR and Scuola Normale Superiore, Piazza San Silvestro 12, I-56127 Pisa, Italy*

(Received 14 November 2020; revised 4 June 2021; accepted 20 July 2021; published 9 August 2021)

Conductance of the edge modes and conductance across the copropagating edge modes around the $\nu = 4/3$, $5/3$, and 2 quantum Hall states are measured by individually exciting the modes. Temperature-dependent equilibration rates of the outer unity conductance edge mode are presented for different filling fractions. We find that the equilibration rate of the outer unity conductance mode at $\nu = 2$ is higher and more temperature sensitive compared to the modes at fractional fillings $5/3$ and $4/3$. At the lowest temperature, the equilibration length of the outer unity conductance mode tends to saturate with the lowering filling fraction ν by increasing the magnetic field B. We speculate this saturating nature of the equilibration length is arising from an interplay of the Coulomb correlation and spin orthogonality.

DOI: 10.1103/PhysRevB.104.085304

I. INTRODUCTION

Quantum Hall (QH) systems formed the first examples of topological insulators, where a set of gapless, topologically protected edge modes carry the current around a bulk region that is gapped due to an interplay of the applied magnetic field and interaction. Robustness of the QH systems has allowed extensive theoretical and experimental investigations of the detailed chiral edge transport revealing rich physics arising along the one-dimensional boundary [1–6]. Though the bulk QH state fixes the total charge conductance along the boundary, the confinement potentials and electronic interactions can reconstruct the edge modes affecting the details of the current distribution [3,7–13]. Robustness and coherence of reconstructed edge modes [14,15] can have implications in the investigation of quantum interferometry [16–18], in braiding statistics [19–22], and in QH circuit designs for quantum electronics applications [23,24]. Weakly equilibrating fractional conductance modes have been realized around $\nu = 1$ [25,26] and $\nu = 2/3$ [5,10,27,28] states, where larger equilibration lengths are achieved in the high magnetic field limit [29]. Characterization of the equilibration processes is thus a question of active interest.

In this work, we focus on equilibration of the spin orthogonal edge modes occurring around states at filling fractions higher than 1, namely, at $\nu = 4/3$, $5/3$, and 2. The $\nu = 4/3$ state is fully spin polarized in Si/SiGe heterostructures [30]. A spin polarization transition can occur in two-dimensional (2D) hole gas [31–33] as well as in 2D electron gas [34] embedded in GaAs/AlGaAs heterostructures under tilted-magnetic-field-induced excess Zeeman splitting. The edge of the spin unpolarized $\nu = 4/3$ QH state in GaAs/AlGaAs heterostructure has two copropagating spin orthogonal charge modes with conductances 1 and $1/3$ [6,35], with equilibration lengths measured up to a few hundred micrometers. The edge structure of the integer QH state at $\nu = 2$ is well understood [36–39], where two unity conductance spin orthogonal copropagating edge modes carry the current. Scattering between the spin orthogonal edge modes can occur through spin flip processes assisted by the dynamics of nuclear spins [40–45]. Current-voltage spectroscopy of the QH states at filling fractions $\nu = 4/3$, $5/3$, 2, and 3 shows that conductance across the copropagating edge modes is enhanced above an interedge mode threshold bias $V_{\rm th}$ and the threshold voltage $V_{\rm th}$ increases with decreasing the filling fraction ν [46]. Above the threshold voltage, conductance across the edge modes reaches the equilibration value for integer filling fractions $\nu = 2$ and 3. In contrast, for fractional fillings $\nu = 5/3$ and $4/3$ the conductance across the modes is below the corresponding equilibrium value above the threshold voltage. Above the threshold voltage $V_{\rm th}$, interedge equilibration becomes faster because of the flat-band scenario [46]. As a consequence, it is difficult to estimate the equilibration length and rate of the edge modes at high imbalance. In this paper, we intend to study the equilibration between the spin orthogonal edge modes in the linear transport regime at filling fractions $\nu = 4/3$, $5/3$, and 2.

In this article, we study conductance of the edge modes and conductance across the copropagating edge modes around the $\nu = 4/3$, $5/3$, and 2 QH states by individually exciting the modes. We measure the length scales over which the outer unity conductance mode (present in all the QH states under study) equilibrates with the inner modes of conductance 1,

*tanmay.maiti@saha.ac.in

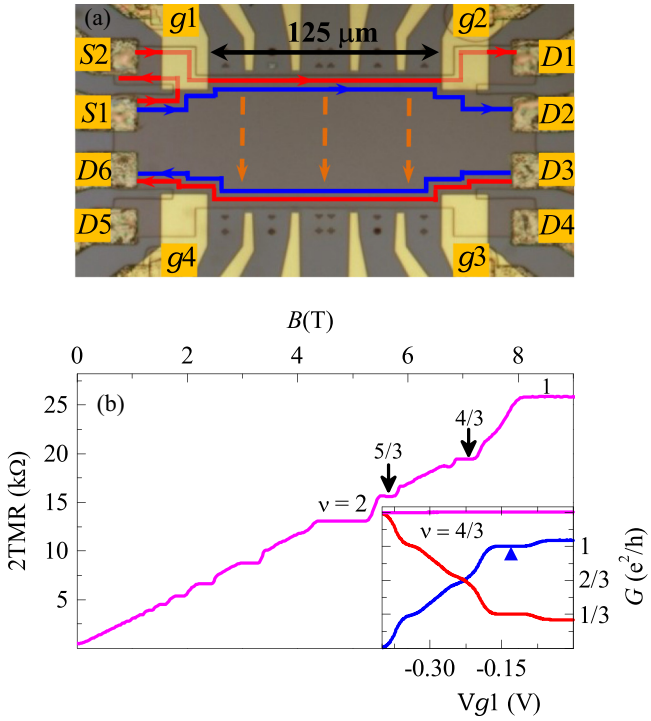

FIG. 1. (a) Optical image of the device used for transport measurement where relevant edge modes for bulk filling fractions $\nu = 4/3$, $5/3$, and 2 are shown. The outer red channel is the unity conductance mode and the blue channel represents the inner mode. Edge modes are separately contacted by setting the filling fraction beneath the two top gates at unity $\nu_1 = \nu_2 = 1$. (b) Two-terminal magnetoresistance trace taken at base temperature. The inset shows $g1$ gate characteristics at filling fraction $\nu = 4/3$ keeping $g2$ under the pinch-off condition, where the blue line represents the transmittance conductance ($S1 \rightarrow S2$), the red line represents the reflected conductance ($S1 \rightarrow D2$), and the magenta line represents the total conductance.

$2/3$, and $1/3$ for the bulk fillings $\nu = 2$, $5/3$, and $4/3$, respectively. We find that the equilibration rate of the outer unity conductance mode at $\nu = 2$ is higher and more temperature sensitive than that of fractional fillings $5/3$ and $4/3$. At the lowest temperature the equilibration length of the outer unity conductance mode shows saturating behavior with increasing the magnetic field B, i.e., decreasing the bulk filling fraction ν. The observation of significantly larger equilibration length in the case of fillings $4/3$ and $5/3$ relative to the $\nu = 2$ case potentially indicates a slower equilibration between an integer and a fractional mode.

II. DEVICE DESCRIPTION AND MEASUREMENT PROCEDURE

Experiments are carried out on a modulation-doped GaAs/AlGaAs heterostructure, in which the two-dimensional electron gas (2DEG) resides at the GaAs/AlGaAs heterointerface located 100 nm below the top surface. Figure 1(a) shows the device structure, where eight ohmic contacts $S1$, $S2$, $D1$, $D2$, $D3$, $D4$, $D5$, and $D6$ are defined for current injection and detection and four top gates $g1$, $g2$, $g3$, and $g4$ are used to tune the filling fraction in the mesa underneath the gates. A customized preamplifier SR555 [29] is deployed at the $S2$ contact to measure output current and for application of AC voltage excitation simultaneously. The device is mounted in a dilution refrigerator equipped with a 14-T superconducting magnet at a base temperature of 7 mK, where the electron temperature achieved is about 30 mK. Carriers are injected by illumination with a GaAs light emitting diode in the sample at 3 K and these carriers are persistent at low temperatures [47]. The carrier density and mobility of the sample become $n \sim 2.27 \times 10^{11}$ cm^{-2} and $\mu \sim 4 \times 10^6$ cm^2/Vs, respectively, after light illumination. Two-terminal magnetoresistance (2TMR) [Fig. 1(b)] is measured to find the location of the QH states, namely, $\nu = 4/3$, $5/3$, and 2 along the magnetic field axis at the base temperature. For our transport experiments at fillings $\nu = 4/3$, $5/3$, and 2 the magnetic fields are set at 7.1, 5.69, and 4.9 T [as indicated in Fig. 1(b)], respectively. The top gates $g3$ and $g4$ are kept at the pinch-off condition by applying a negative voltage bias of $Vg3 = Vg4 = -0.450$ V throughout the experiment.

We set the magnetic field at 7.1 T to carry out top gate $g1$ characteristics at the bulk filling fraction $\nu = 4/3$ keeping the top gate $g2$ in the pinch-off condition. Transmitted and reflected conductances are measured between $S1 \rightarrow S2$ and $S1 \rightarrow D2$, respectively, by varying the top gate voltage $Vg1$ as shown in the inset of Fig. 1(b).The transmitted conductance (blue curve) shows a plateau at unit conductance, confirming the formation of an integer QH state of the filling $\nu_1 = 1$ beneath the top gate $g1$ within a gate voltage range of -0.168 to -0.099 V. The red curve represents the reflected conductance and the magenta curve shows the total conductance. The total conductance remains constant at $4/3$ throughout the gate voltage $Vg1$ scan, confirming conservation of the current. A similar gate characteristic is also observed for the top gate $g2$ at the bulk filling $\nu = 4/3$. From the gate characteristics, we can determine the gate voltage range in which an integer QH state of filling unity is formed beneath the gates $g1$ and $g2$. Similarly, gate voltage ranges of top gates $g1$ and $g2$ are found to set the filling fraction unity $\nu_1 = \nu_2 = 1$ beneath the gates at bulk filling fractions $\nu = 5/3$ and 2.

III. EXPERIMENTAL RESULTS AND ANALYSIS

Upon setting $\nu_1 = \nu_2 = 1$ beneath the gates, we separately contact the edge modes for selective current injection and detection [39,48] in the $\nu = 4/3$, $5/3$, and 2 QH states. In this device, the outer unity conductance mode (red line) connects $S2$ to $D1$, and $S1$ is connected to $D2$ by the inner edge mode (blue line) with conductances $1/3$, $2/3$, and 1 for filling fractions $\nu = 4/3$, $5/3$, and 2, respectively [3,6], as shown in Fig. 1(a). To understand the equilibration between these edge modes, we perform the temperature-dependent transport measurements from 30 mK to only 500 mK, preventing thermal degradation of the sample—loss of carriers and reduction of mobility. During the temperature-dependence experiment, $S1$ and $S2$ are excited with $V_{S1} = 25.8$ μV (17 Hz) and $V_{S2} = 25.8$ μV (26 Hz), and currents at $D1$ and $D2$ are measured with the two frequency windows and backscattered current (17 Hz) is measured at $D6$. With this excitation voltage, we work in the linear transport regime. We define the measured quantities ${}^{\nu}G_{S\rightarrow D}$, which denote two-terminal conductance

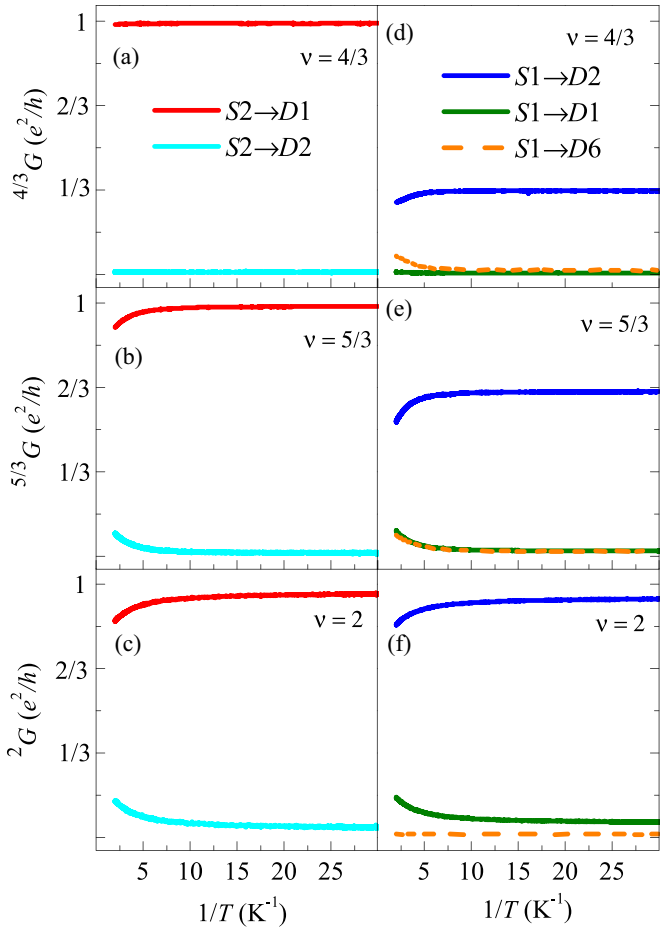

FIG. 2. Two-terminal conductances as a function of $1/T$, when S2 is excited with 25.8 μV at 26 Hz for bulk filling fractions (a) $\nu = 4/3$, (b) $\nu = 5/3$, and (c) $\nu = 2$. Two-terminal conductances as a function of $1/T$ when $S1$ is excited with 25.8 μV at 17 Hz for (d) $\nu = 4/3$, (e) $\nu = 5/3$, and (f) $\nu = 2$.

(TTC) between a source S and a drain D at the bulk filling fraction ν, while filling fractions $\nu_1 = \nu_2 = 1$ are maintained under the gates. The TTC ${}^{\nu}G_{S\to D}$ can also be expressed in terms of transmission probabilities of the copropagating edge modes (see Appendix A).

Temperature-dependent TTCs are presented in Fig. 2. At the filling fraction $\nu = 4/3$, TTCs between contacts $S2 \to D1$ and $S2 \to D2$ are shown in Fig. 2(a) by the red and cyan curves, respectively. With increasing temperature up to 500 mK, we see that TTC ${}^{4/3}G_{S2\to D1}$ stays fixed to 1 and zero conductance is measured for TTC ${}^{4/3}G_{S2\to D2}$, indicating no measurable equilibration between the outer unity conductance mode and the inner 1/3 conductance mode up to 500 mK over a propagation length of $l = 125$ μm. Similar temperature-dependent experiments for filling fractions $\nu = 5/3$ and 2 show that, with increasing temperature, ${}^{5/3}G_{S2\to D1}$ and ${}^{2}G_{S2\to D1}$ decrease [red curve in Figs. 2(b) and 2(c)] while ${}^{5/3}G_{S2\to D2}$ and ${}^{2}G_{S2\to D2}$ increase [cyan curve in Figs. 2(b) and 2(c)]. The compensating nature of the conductances confirms the conservation of current. At higher temperatures, the outer unity conductance mode equilibrates with inner 2/3 and 1 conductance modes for bulk filling fractions $\nu = 5/3$ and 2, respectively. Suppression of intermode scattering over the propagation length of $l = 125$ μm is evident in Figs. 2(a)–2(c) at the lowest temperature accessible in our experiments.

The TTC ${}^{4/3}G_{S1\to D2}$ decreases with increasing temperature as shown in Fig. 2(d) (blue curve) while ${}^{4/3}G_{S1\to D1}$ (olive curve) remains fixed to zero due to the absence of equilibration up to 500 mK, as also seen for ${}^{4/3}G_{S2\to D2}$ in Fig. 2(a). The TTC for the current reaching at $D6$ from $S1$ increases with increasing temperature [dashed orange curve of Fig. 2(d)], indicating backscattering of the inner 1/3 edge mode into the oppositely moving edge channel across the bulk [Fig. 1(a)]. For the filling fraction $\nu = 5/3$ in the bulk, TTC ${}^{5/3}G_{S1\to D2}$ (${}^{5/3}G_{S1\to D1}$) decreases (increases) with increasing temperature as shown in Fig. 2(e) by the blue (olive) curve, and the backscattered current at $D6$ also increases [dashed orange curve of Fig. 2(e)] with increasing temperature. The observation indicates simultaneous equilibration of copropagating modes and backscattering of the 2/3 mode with increasing temperature. At the bulk filling fraction $\nu = 2$, decrease of ${}^{2}G_{S1\to D2}$ is fully compensated by increase of ${}^{2}G_{S1\to D1}$, and no current reaches at $D6$ [Fig. 2(f)], which confirms the incompressibility of the QH state at $\nu = 2$ within the range of temperature variations. At filling fractions $\nu = 4/3$ and 5/3, the sub-Kelvin bulk gaps (see Appendix B) originate from the Coulomb interaction, while the bulk gap at the filling fraction $\nu = 2$ is the Landau gap $\hbar\omega_c$ (ω_c, cyclotron frequency). Hence, breakdown of the QH state at $\nu = 2$ is not observed, as the cyclotron gap $\hbar\omega_c$ is much larger than the maximum applied thermal excitation kT ($T = 500$ mK).

To quantify the temperature dependence of the equilibration process between the edge modes, we define the equilibration length l_r of the outer integer edge mode, where $1/l_r$ is the rate of charge transfer from the outer mode to the inner mode. The corresponding TTC of the outer mode connecting $S2$ to $D1$ can be written as [29,37,48–50]

$$ {}^{2}G_{S2\to D1} = \tfrac{1}{2}[1 + e^{-2l/l_r}], \tag{1}$$

for $\nu = 2$, where the prefactors are fixed by the boundary conditions—no scattering into inner modes at $l = 0$ and full equilibration at $l \gg l_r$. Similarly, the TTC at filling fractions $\nu = 4/3$ and 5/3 can be written as [29]

$$ {}^{4/3}G_{S2\to D1} = \tfrac{1}{4}[3 + e^{-4l/l_r}] \tag{2}$$

and

$$ {}^{5/3}G_{S2\to D1} = \tfrac{1}{5}[3 + 2e^{-5l/2l_r}], \tag{3}$$

respectively. The above equations are utilized to estimate the value of the equilibration rate $1/l_r$ from the measured TTC between the contacts $S2$ to $D1$ in Figs. 2(a), 2(b), and 2(c) (red curves). It is assumed that the small amount of current that backscatters from the inner mode does not alter the above relations.

The equilibration rate $1/l_r$ of the outer integer mode is plotted as a function of $1/T$ in Fig. 3(a) for filling fractions $\nu = 4/3$, 5/3, and 2. At the filling fraction $\nu = 1.45$ the QH state is compressible where the inner mode does not exist; however, an effective equilibration rate can be estimated for the outer mode using a similar exponential formulation, and this shows an intermediate value as shown in Fig. 3(a). The equilibration rates for all the filling fractions increase monotonically with increasing temperature. The equilibration rates

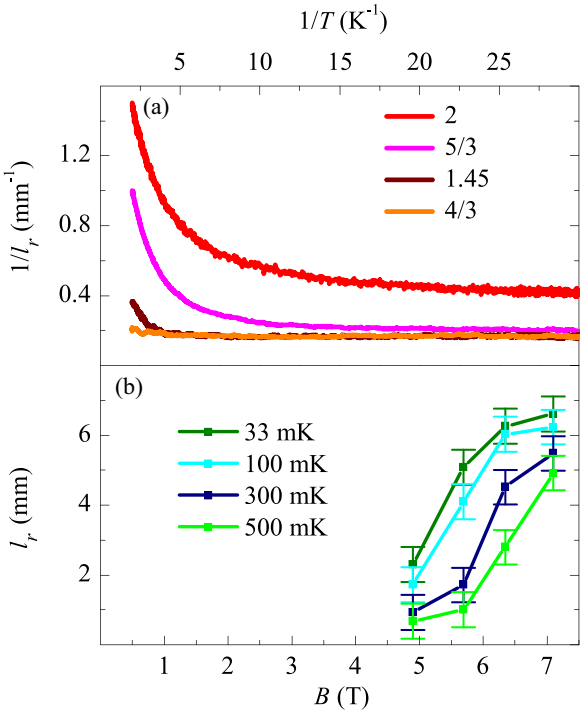

FIG. 3. (a) Equilibration rate of the outer unity conductance mode versus $1/T$ at $\nu = 4/3$, 1.45, 5/3, and 2. (b) Plot of equilibration length versus B for different temperatures.

for fractional fillings $\nu = 4/3$ and $5/3$ are similar at the lowest temperature, but distinctly lower than that of the integer filling $\nu = 2$. To understand this observation at the lowest temperature, the equilibration length of the outer unity conductance mode is estimated to be 6.6 ± 0.5, 6.3 ± 0.5, 5.1 ± 0.5, and 2.3 ± 0.5 mm for filling fractions $\nu = 4/3$, 1.45, 5/3, and 2, respectively, and is plotted with magnetic field in Fig. 3(b). The equilibration length l_r tends to saturate with increasing magnetic field (i.e., lowering the filling fraction ν) at the lowest temperature, and with increasing temperature the saturating trend of l_r disappears [Fig. 3(b)].

IV. DISCUSSION

Edge mode structures of the QH states along smooth boundaries arise from formation of a sequence of dominant incompressible states as the electron density changes from the bulk value to zero at the boundary [3,51]. Here, two spatially separated edge modes are formed by incompressibility due to spin gap, and the spin orthogonality condition prevents equilibration between these modes at the lowest temperature. Therefore, the equilibration process requires a spin flip mechanism that is mediated by dynamic nuclear polarization [40–44].

Spin polarization of the QH system increases with lowering the bulk filling fraction ν below 2, and the QH system becomes fully spin polarized at the filling $\nu = 1$. This change of the spin polarization from spin unpolarized ($\nu = 2$) to spin polarized ($\nu = 1$) results in exchange enhancement of the g factor with lowering the filling fraction [52,53]. The enhanced spin gap is reflected in the observation of increase of the threshold voltage $V_{\rm th}$ for intermode transport with lowering filling fractions $\nu = 2$ to $4/3$ [46]. The exchange-enhanced spin gap induces spatial separation of the opposite spin modes. As a consequence of the increase in spatial separation, the equilibration length l_r should increase with increasing magnetic field without showing saturation [29]. In contrast, the measured equilibration length l_r of the outer unity conductance mode tends to saturate with increasing magnetic field B as shown in Fig. 3(b) at the lowest temperature.

In addition to the spin orthogonality, the equilibration process may also be suppressed due to differing character of the electronlike quasiparticles in the outer unity conductance mode and the anyonlike quasiparticles in the correlated inner mode of $\nu = 5/3$ and $4/3$ [54]. This could explain the significantly larger equilibration rates in the integer QH state at $\nu = 2$ as compared to the fractional QH states at asymptotically low temperatures. A quantitative modeling of the observed saturating nature of the equilibration length l_r is left for further investigations.

V. CONCLUSION

In conclusion, we study equilibration between pairs of copropagating edge modes of conductance 1 on the outer side and $\nu - 1$ on the inner side for bulk filling fractions $\nu = 2$, $5/3$, and $4/3$. We observe the saturating nature of the equilibration length l_r of the outer unity conductance mode with increasing magnetic field at the lowest temperature. We argue that the significantly larger equilibration length for fillings $\nu = 5/3$ and $4/3$ compared to the filling $\nu = 2$ arises from suppression of equilibration due to differing character of the electronlike quasiparticles in the outer unity conductance mode and the anyonlike quasiparticles in the correlated inner mode.

ACKNOWLEDGMENTS

G.J.S. acknowledges support from DST-SERB Grant No. ECR/2018/001781. Part of the discussions in this and related previous works were facilitated by the International Centre for Theoretical Sciences program on Edge Dynamics in Topological Phases (ICTS/edytop2019/06). S.D. acknowledges support from DST-SERB Grant No. MTR/2019/001043 and an ARF grant from IISER Kolkata.

APPENDIX A

In our experiments, the two-terminal conductance (TTC) ${}^{\nu}G_{S\to D}$ is measured in a multiterminal device as shown in Fig. 1(a). The measured TTC ${}^{\nu}G_{S\to D}$ can be expressed in terms of transmission probabilities of the copropagating edge modes connecting the source and the detector. For this representation the outer mode and the inner mode are labeled 1 and 2, respectively, where the outer mode has conductance unity and the inner mode has conductances 1, 2/3, and 1/3 for bulk filling fractions $\nu = 2$, $5/3$, and $4/3$, respectively. Following Büttiker's approach [3,29,55] the TTC for the bulk filling fraction ν can be expressed as

$$ {}^{\nu}G_{\rm S\to D} = \sum_{i;j} g_i T_{ij}, \tag{A1}$$

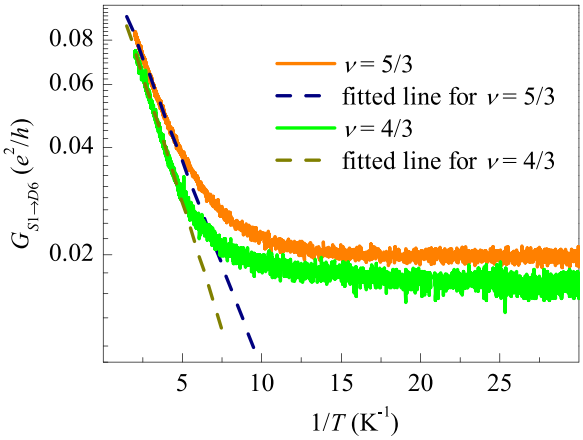

FIG. 4. Arrhenius plot of the backscattered conductance at fillings $\nu = 4/3$ and $5/3$.

where T_{ij} represents the probability of transmission from mode i connected to the source S into mode j connected to the detector D. The summation $i(j)$ is taken over all the modes connected to the source (detector). g_i is conductance of the ith mode connected to the source S. The transmission probability T_{ij} between the respective modes depends on the charge equilibration over the copropagation length $l = 125$ μm. In this presentation we exclude backscattered current reaching to detector $D6$.

Now we focus on the bulk filling fraction $\nu = 4/3$, where the TTCs can be expressed as

$$^{4/3}G_{S2\to D1} = T_{11}, \tag{A2}$$

$$^{4/3}G_{S2\to D2} = T_{12}, \tag{A3}$$

$$^{4/3}G_{S1\to D2} = \tfrac{1}{3}T_{22}, \tag{A4}$$

$$^{4/3}G_{S1\to D1} = \tfrac{1}{3}T_{21}. \tag{A5}$$

At the lowest temperature, the two copropagating modes do not equilibrate; hence, the values of transmission probabilities become $T_{11} = T_{22} = 1, T_{12} = T_{21} = 0$. With increasing temperature, the two copropagating modes start equilibration into each other. If they fully equilibrate, the transmission probabilities become $T_{11} = 3/4$, $T_{12} = 1/4$, $T_{22} = 1/4$, and $T_{21} = 3/4$. In our experiment, the temperature dependence of the TTCs is plotted in Figs. 2(a) and 2(d) for the filling fraction $\nu = 4/3$. The equilibration rate $1/l_r$ of the outer unity conductance mode for $\nu = 4/3$ is calculated using Eq. (2) from the measured value of T_{11} [Eq. (A2)]. Similarly, TTCs at other filling fractions $\nu = 5/3$ and 2 can also be expressed.

APPENDIX B

In general, insulating states at the bulk gap melt at higher temperatures and start conducting, resulting in backscattering of the edge modes as depicted in Fig. 1(a) (orange dashed lines). In our device, backscattered current reaches the contact $D6$ when source $S1$ is excited, and the corresponding TTC $^{\nu}G_{S1\to D6}$ increases with increasing temperature as shown in Fig. 2(d) for $\nu = 4/3$ and in Fig. 2(e) for $\nu = 5/3$ (orange curves). In a Hall bar device, the characteristic bulk gap is estimated from the Arrhenius plot of the finite longitudinal resistivity at elevated temperatures. A similar activation behavior is seen in our temperature-dependent measurement [Figs. 2(d) and 2(e)], in which TTC from $S1$ to $D6$ can be expressed as [56–58]

$$^{\nu}G_{S1\to D6} \propto e^{-\frac{\Delta_\nu}{2T}}, \tag{B1}$$

where Δ_ν is the bulk energy gap (also call pair creation energy) at the filling fraction ν. The backscattered conductance ($S1$ to $D6$) for filling fractions $\nu = 4/3$ and $5/3$ are presented in Fig. 4. The high-temperature part of the data is fitted linearly to estimate the bulk gap and is found to be $\Delta_{4/3} = 0.652 \pm 0.06$ K and $\Delta_{5/3} = 0.534 \pm 0.06$ K for filling fractions $\nu = 4/3$ and $5/3$, respectively. The measured bulk gaps are consistent with the previous measurements [56,57].

[1] A. M. Chang, Chiral Luttinger liquids at the fractional quantum Hall edge, Rev. Mod. Phys. **75**, 1449 (2003).

[2] A. H. MacDonald, Edge States in the Fractional-Quantum-Hall-Effect Regime, Phys. Rev. Lett. **64**, 220 (1990).

[3] C. W. J. Beenakker, Edge Channels for the Fractional Quantum Hall Effect, Phys. Rev. Lett. **64**, 216 (1990).

[4] Y. Meir, Composite Edge States in the $\nu = 2/3$ Fractional Quantum Hall Regime, Phys. Rev. Lett. **72**, 2624 (1994).

[5] R. Sabo, I. Gurman, A. Rosenblatt, F. Lafont, D. Banitt, J. Park, M. Heiblum, Y. Gefen, V. Umansky, and D. Mahalu, Edge reconstruction in fractional quantum Hall states, Nat. Phys. **13**, 491 (2017).

[6] C. Lin, R. Eguchi, M. Hashisaka, T. Akiho, K. Muraki, and T. Fujisawa, Charge equilibration in integer and fractional quantum Hall edge channels in a generalized Hall-bar device, Phys. Rev. B **99**, 195304 (2019).

[7] C. de C. Chamon and X. G. Wen, Sharp and smooth boundaries of quantum Hall liquids, Phys. Rev. B **49**, 8227 (1994).

[8] G. Kirczenow and B. L. Johnson, Composite fermions, edge currents, and the fractional quantum Hall effect, Phys. Rev. B **51**, 17579 (1995).

[9] X. Wan, K. Yang, and E. H. Rezayi, Reconstruction of Fractional Quantum Hall Edges, Phys. Rev. Lett. **88**, 056802 (2002).

[10] J. Wang, Y. Meir, and Y. Gefen, Edge Reconstruction in the $\nu = 2/3$ Fractional Quantum Hall State, Phys. Rev. Lett. **111**, 246803 (2013).

[11] X. Wan, E. H. Rezayi, and K. Yang, Edge reconstruction in the fractional quantum Hall regime, Phys. Rev. B **68**, 125307 (2003).

[12] Y. N. Joglekar, H. K. Nguyen, and G. Murthy, Edge reconstructions in fractional quantum Hall systems, Phys. Rev. B **68**, 035332 (2003).

[13] K. Yang, Field Theoretical Description of Quantum Hall Edge Reconstruction, Phys. Rev. Lett. **91**, 036802 (2003).

[14] Y. Ronen, Y. Cohen, D. Banitt, M. Heiblum, and V. Umansky, Robust integer and fractional helical modes in the quantum Hall effect, Nat. Phys. **14**, 411 (2018).

[15] J. Nakamura, S. Fallahi, H. Sahasrabudhe, R. Rahman, S. Liang, G. C. Gardner, and M. J. Manfra, Aharonov–Bohm interference of fractional quantum Hall edge modes, Nat. Phys. **15**, 563 (2019).

[16] D. T. McClure, W. Chang, C. M. Marcus, L. N. Pfeiffer, and K. W. West, Fabry-Perot Interferometry with Fractional Charges, Phys. Rev. Lett. **108**, 256804 (2012).

[17] N. Ofek, A. Bid, M. Heiblum, A. Stern, V. Umansky, and D. Mahalu, Role of interactions in an electronic Fabry–Perot interferometer operating in the quantum Hall effect regime, Proc. Natl. Acad. Sci. U.S.A. **107**, 5276 (2010).

[18] J. Park, Y. Gefen, and H.-S. Sim, Topological dephasing in the $\nu = 2/3$ fractional quantum Hall regime, Phys. Rev. B **92**, 245437 (2015).

[19] J. Nakamura, S. Liang, G. Gardner, and M. Manfra, Direct observation of anyonic braiding statistics, Nat. Phys. **16**, 931 (2020).

[20] B. I. Halperin, Statistics of Quasiparticles and the Hierarchy of Fractional Quantized Hall States, Phys. Rev. Lett. **52**, 1583 (1984).

[21] E.-A. Kim, Aharanov-Bohm Interference and Fractional Statistics in a Quantum Hall Interferometer, Phys. Rev. Lett. **97**, 216404 (2006).

[22] D. Arovas, J. R. Schrieffer, and F. Wilczek, Fractional Statistics and the Quantum Hall Effect, Phys. Rev. Lett. **53**, 722 (1984).

[23] Y. Ji, Y. Chung, D. Sprinzak, M. Heiblum, D. Mahalu, and H. Shtrikman, An electronic Mach–Zehnder interferometer, Nature (London) **422**, 415 (2003).

[24] I. Neder, N. Ofek, Y. Chung, M. Heiblum, D. Mahalu, and V. Umansky, Interference between two indistinguishable electrons from independent sources, Nature (London) **448**, 333 (2007).

[25] L. P. Kouwenhoven, B. J. van Wees, N. C. van der Vaart, C. J. P. M. Harmans, C. E. Timmering, and C. T. Foxon, Selective Population and Detection of Edge Channels in the Fractional Quantum Hall Regime, Phys. Rev. Lett. **64**, 685 (1990).

[26] R. Bhattacharyya, M. Banerjee, M. Heiblum, D. Mahalu, and V. Umansky, Melting of Interference in the Fractional Quantum Hall Effect: Appearance of Neutral Modes, Phys. Rev. Lett. **122**, 246801 (2019).

[27] C. Nosiglia, J. Park, B. Rosenow, and Y. Gefen, Incoherent transport on the $\nu = 2/3$ quantum Hall edge, Phys. Rev. B **98**, 115408 (2018).

[28] Y. Gross, M. Dolev, M. Heiblum, V. Umansky, and D. Mahalu, Upstream Neutral Modes in the Fractional Quantum Hall Effect Regime: Heat Waves or Coherent Dipoles, Phys. Rev. Lett. **108**, 226801 (2012).

[29] T. Maiti, P. Agarwal, S. Purkait, G. J. Sreejith, S. Das, G. Biasiol, L. Sorba, and B. Karmakar, Magnetic-Field-Dependent Equilibration of Fractional Quantum Hall Edge Modes, Phys. Rev. Lett. **125**, 076802 (2020).

[30] K. Lai, W. Pan, D. C. Tsui, and Y.-H. Xie, Fractional quantum Hall effect at $\nu = \frac{2}{3}$ and $\frac{4}{3}$ in strained Si quantum wells, Phys. Rev. B **69**, 125337 (2004).

[31] A. G. Davies, R. Newbury, M. Pepper, J. E. F. Frost, D. A. Ritchie, and G. A. C. Jones, Fractional quantum Hall effect in high-mobility two-dimensional hole gases in tilted magnetic fields, Phys. Rev. B **44**, 13128 (1991).

[32] P. J. Rodgers, B. L. Gallagher, M. Henini, and G. Hill, Observation of a spin polarization phase transition of the 4/3 fractional quantum Hall state in a high-mobility 2D hole system, J. Phys.: Condens. Matter **5**, L565 (1993).

[33] K. Muraki and Y. Hirayama, Re-entrant behavior of the $\nu = 4/3$ fractional quantum Hall effect in a front-and-back-gated 2D hole gas, Phys. B: Condens. Matter **256-258**, 86 (1998).

[34] R. G. Clark, S. R. Haynes, A. M. Suckling, J. R. Mallett, P. A. Wright, J. J. Harris, and C. T. Foxon, Spin Configurations and Quasiparticle Fractional Charge of Fractional-Quantum-Hall-Effect Ground States in the $n = 0$ Landau Level, Phys. Rev. Lett. **62**, 1536 (1989).

[35] C. Altimiras, H. le Sueur, U. Gennser, A. Anthore, A. Cavanna, D. Mailly, and F. Pierre, Chargeless Heat Transport in the Fractional Quantum Hall Regime, Phys. Rev. Lett. **109**, 026803 (2012).

[36] B. I. Halperin, Quantized Hall conductance, current-carrying edge states, and the existence of extended states in a two-dimensional disordered potential, Phys. Rev. B **25**, 2185 (1982).

[37] G. Müller, D. Weiss, A. V. Khaetskii, K. von Klitzing, S. Koch, H. Nickel, W. Schlapp, and R. Lösch, Equilibration length of electrons in spin-polarized edge channels, Phys. Rev. B **45**, 3932 (1992).

[38] W. Kang, H. Stormer, L. Pfeiffer, K. Baldwin, and K. West, Tunnelling between the edges of two lateral quantum Hall systems, Nature (London) **403**, 59 (2000).

[39] B. Karmakar, D. Venturelli, L. Chirolli, F. Taddei, V. Giovannetti, R. Fazio, S. Roddaro, G. Biasiol, L. Sorba, V. Pellegrini, and F. Beltram, Controlled Coupling of Spin-Resolved Quantum Hall Edge States, Phys. Rev. Lett. **107**, 236804 (2011).

[40] T. Machida, S. Ishizuka, T. Yamazaki, S. Komiyama, K. Muraki, and Y. Hirayama, Spin polarization of fractional quantum Hall edge channels studied by dynamic nuclear polarization, Phys. Rev. B **65**, 233304 (2002).

[41] K. Yang, K. Nagase, Y. Hirayama, T. D. Mishima, M. B. Santos, and H. Liu, Role of chiral quantum Hall edge states in nuclear spin polarization, Nat. Commun. **8**, 15084 (2017).

[42] B. E. Kane, L. N. Pfeiffer, and K. W. West, Evidence for an electric-field-induced phase transition in a spin-polarized two-dimensional electron gas, Phys. Rev. B **46**, 7264 (1992).

[43] K. R. Wald, L. P. Kouwenhoven, P. L. McEuen, N. C. van der Vaart, and C. T. Foxon, Local Dynamic Nuclear Polarization Using Quantum Point Contacts, Phys. Rev. Lett. **73**, 1011 (1994).

[44] D. C. Dixon, K. R. Wald, P. L. McEuen, and M. R. Melloch, Dynamic nuclear polarization at the edge of a two-dimensional electron gas, Phys. Rev. B **56**, 4743 (1997).

[45] E. V. Deviatov, A. Würtz, A. Lorke, M. Yu. Melnikov, V. T. Dolgopolov, D. Reuter, and A. D. Wieck, Two relaxation mechanisms observed in transport between spin-split edge states at high imbalance, Phys. Rev. B **69**, 115330 (2004).

[46] E. V. Deviatov, A. Lorke, and W. Wegscheider, Manifestation of a complex edge excitation structure in the quantum Hall regime at high fractional filling factors, Phys. Rev. B **78**, 035310 (2008).

[47] M. I. Nathan, Persistent photoconductivity in AlGaAs/GaAs modulation doped layers and field effect transistors: A review, Solid-State Electron. **29**, 167 (1986).

[48] A. Würtz, R. Wildfeuer, A. Lorke, E. V. Deviatov, and V. T. Dolgopolov, Separately contacted edge states: A spectroscopic tool for the investigation of the quantum Hall effect, Phys. Rev. B **65**, 075303 (2002).

[49] Y. Takagaki, K. J. Friedland, J. Herfort, H. Kostial, and K. Ploog, Inter-edge-state scattering in the spin-polarized quantum Hall regime with current injection into inner states, Phys. Rev. B **50**, 4456 (1994).

[50] N. Paradiso, S. Heun, S. Roddaro, D. Venturelli, F. Taddei, V. Giovannetti, R. Fazio, G. Biasiol, L. Sorba, and F. Beltram, Spatially resolved analysis of edge-channel equilibration in quantum Hall circuits, Phys. Rev. B **83**, 155305 (2011).

[51] D. B. Chklovskii, B. I. Shklovskii, and L. I. Glazman, Electrostatics of edge channels, Phys. Rev. B **46**, 4026 (1992).

[52] V. T. Dolgopolov, A. A. Shashkin, A. V. Aristov, D. Schmerek, W. Hansen, J. P. Kotthaus, and M. Holland, Direct Measurements of the Spin Gap in the Two-Dimensional Electron Gas of AlGaAs-GaAs Heterojunctions, Phys. Rev. Lett. **79**, 729 (1997).

[53] D. Werner and J. Oswald, Size scaling of the exchange interaction in the quantum Hall effect regime, Phys. Rev. B **102**, 235305 (2020).

[54] U. Zülicke, J. J. Palacios, and A. H. MacDonald, Fractional-quantum-Hall edge electrons and Fermi statistics, Phys. Rev. B **67**, 045303 (2003).

[55] M. Büttiker, Absence of backscattering in the quantum Hall effect in multiprobe conductors, Phys. Rev. B **38**, 9375 (1988).

[56] G. S. Boebinger, H. L. Stormer, D. C. Tsui, A. M. Chang, J. C. M. Hwang, A. Y. Cho, C. W. Tu, and G. Weimann, Activation energies and localization in the fractional quantum Hall effect, Phys. Rev. B **36**, 7919 (1987).

[57] G. S. Boebinger, A. M. Chang, H. L. Stormer, and D. C. Tsui, Magnetic Field Dependence of Activation Energies in the Fractional Quantum Hall Effect, Phys. Rev. Lett. **55**, 1606 (1985).

[58] R. L. Willett, H. L. Stormer, D. C. Tsui, A. C. Gossard, and J. H. English, Quantitative experimental test for the theoretical gap energies in the fractional quantum Hall effect, Phys. Rev. B **37**, 8476 (1988).